NASA TECHNICAL NOTE
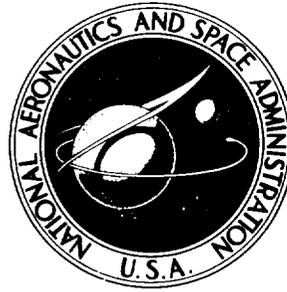
NASA TN D-8244

PREDICTING FAILURE OF SPECIMENS WITH EITHER SURFACE CRACKS OR CORNER CRACKS AT HOLES

J. C. Newman, Jr.

Langley Research Center
Hampton, Va. 23665

NATIONAL AERONAUTICS AND SPACE ADMINISTRATION • WASHINGTON, D. C. • JUNE 1976

1. Report No. NASA TN D-8244	2. Government Accession No.	3. Recipient's Catalog No.
4. Title and Subtitle PREDICTING FAILURE OF SPECIMENS WITH EITHER SURFACE CRACKS OR CORNER CRACKS AT HOLES		5. Report Date June 1976
		6. Performing Organization Code
7. Author(s) J. C. Newman, Jr.		8. Performing Organization Report No. L-10203
		10. Work Unit No. 505-02-31-01
9. Performing Organization Name and Address NASA Langley Research Center Hampton, Va. 23665		11. Contract or Grant No.
		13. Type of Report and Period Covered Technical Note
12. Sponsoring Agency Name and Address National Aeronautics and Space Administration Washington, D.C. 20546		14. Sponsoring Agency Code

15. Supplementary Notes

16. Abstract

    A previously developed fracture criterion was applied to fracture data for surface-cracked specimens subjected to remote tensile loading and for specimens with a corner crack (or cracks) emanating from a circular hole subjected to either remote tensile loading or pin loading in the hole. The failure stresses calculated from this criterion were consistent with experimental failure stresses for both surface and corner cracks for a wide range of crack shapes and crack sizes in specimens of aluminum alloy, titanium alloy, and steel.

    Empirical equations for the elastic stress-intensity factors for a surface crack and for a corner crack (or cracks) emanating from a circular hole in a finite-thickness and finite-width specimen were also developed.

17. Key Words (Suggested by Author(s)) Crack Stress-intensity factor Materials, metallic Fracture strength	18. Distribution Statement Unclassified – Unlimited Subject Category 39

19. Security Classif. (of this report) Unclassified	20. Security Classif. (of this page) Unclassified	21. No. of Pages 37	22. Price* $3.75

PREDICTING FAILURE OF SPECIMENS WITH EITHER
SURFACE CRACKS OR CORNER CRACKS AT HOLES

J. C. Newman, Jr.
Langley Research Center

SUMMARY

A previously developed fracture criterion was applied to fracture data for surface-cracked specimens subjected to remote tensile loading and for specimens with a corner crack (or cracks) emanating from a circular hole subjected to either remote tensile loading or pin loading in the hole. The failure stresses calculated from this criterion were consistent with experimental failure stresses for both surface and corner cracks for a wide range of crack shapes and crack sizes in specimens of aluminum alloy, titanium alloy, and steel.

Empirical equations for the elastic stress-intensity factors for a surface crack and for a corner crack (or cracks) emanating from a circular hole in a finite-thickness and finite-width specimen were also developed.

INTRODUCTION

Failures of many aircraft and aerospace vehicle components have been traced to surface cracks. Such cracks initiate at structural discontinuities such as holes, material defects, or other abrupt changes in configuration and may propagate to failure under operating stress levels. In designing against these failures, the designer must be able to predict the effects of crack size and shape on structural strength. Linear elastic fracture mechanics (LEFM), which utilizes the concept of elastic stress-intensity factors, has been used to correlate fracture data and to predict failure for cracked plates and structural components when the crack-tip plastic deformations are constrained to small regions (plane-strain fracture (ref. 1)). However, when plastic deformations near the crack tip are large, the elastic stress-intensity factor at failure $K_{I,e}$ varies with planar dimensions, such as crack size and specimen width. (See refs. 2 to 6.) To account for the variation in $K_{I,e}$ with crack size and specimen width, the elastic-plastic—stress-strain behavior at the crack tip must be considered.

An equation which includes the effects of plastic deformation on fracture was derived in references 4 and 5. This equation relates $K_{I,e}$ to the elastic nominal failure stress

and two material fracture parameters and is designated the two-parameter fracture criterion (TPFC). The TPFC was applied to surface-cracked and through-cracked sheet and plate specimens subjected to tensile loading in reference 4 and to compact and notch-bend fracture specimens in reference 5. Reference 6 has also shown that fracture data from one specimen type and the TPFC can be used to predict failure of other specimen types.

In the present paper the TPFC was applied to surface-crack specimens subjected to remote tensile loading and to corner-crack (surface crack or cracks emanating from a circular hole) specimens subjected to either remote tensile loading or pin loading (see fig. 1). Fracture data from the literature on several aluminum and titanium alloys and one steel (refs. 7 to 10) were analyzed.

Previous solutions for the elastic stress-intensity factors for surface cracks and corner cracks at holes either were restricted to limited ranges of crack shape and crack size or were presented in graphical form. To eliminate some of the restrictions and for ease of computation, empirical equations which approximate the elastic stress-intensity factors for a surface crack and for a corner crack (or cracks) in a finite-thickness and finite-width specimen were developed. These equations are compared with other theoretical and experimental stress-intensity factors from the literature.

SYMBOLS

a	initial depth of surface or corner crack, m
b	number of cracks emanating from hole (1 or 2)
c	initial half-length of surface crack or initial length of corner crack at hole, m
c'	initial half-length of through crack (see fig. 13), m
D	hole diameter, m
F	complete boundary correction factor on stress intensity
f_b	Bowie correction factor on stress intensity for through crack (or cracks) at hole
f_w	finite-width correction factor on stress intensity
K_F	fracture toughness computed from equation (1), $N/m^{3/2}$

2

K_I Mode I elastic stress-intensity factor, $N/m^{3/2}$

$K_{I,b}$ Bowie stress-intensity factor (Mode I) for through crack emanating from hole, $N/m^{3/2}$

$K_{I,e}$ Mode I elastic stress-intensity factor at failure, $N/m^{3/2}$

$K_{I,h}$ experimental stress-intensity factor (Mode I) at intersection of crack and hole, $N/m^{3/2}$

$K_{I,s}$ experimental stress-intensity factor (Mode I) at intersection of crack and plate surface, $N/m^{3/2}$

$K_{I,pp}$ stress-intensity factor (Mode I) for crack subjected to pair of wedge force loads, $N/m^{3/2}$

$K_{I,ss}$ stress-intensity factor (Mode I) for crack subjected to uniform stress, $N/m^{3/2}$

$K_{I,sp}$ stress-intensity factor (Mode I) for crack subjected to single wedge force load and uniform stress, $N/m^{3/2}$

M_e combined front-face, back-face, and finite-width correction factor on stress intensity for surface or corner crack

M_1 front-face boundary correction factor on stress intensity for surface or corner crack

m fracture-toughness parameter

P pin load at failure, N

Q elastic surface-crack shape factor

S gross section stress at failure, Pa

S_n nominal (net section) stress at failure, Pa

S_u nominal stress required to produce fully plastic region on net section, Pa

T	temperature, K
t	specimen thickness, m
W	specimen width, m
x	distance from center line of crack to location of wedge force load, m
θ	angle measured from plate surface to point on surface-crack or corner-crack boundary (see insert in fig. 10)
σ_u	ultimate tensile strength, Pa
σ_{ys}	yield stress, Pa

TWO-PARAMETER FRACTURE CRITERION

The two-parameter fracture criterion (TPFC) developed and applied in references 4 to 6 accounts for the effects of plastic deformation on fracture properties and relates the elastic stress-intensity factor at failure $K_{I,e}$, the nominal (net section) failure stress S_n, and two material fracture parameters K_F and m. The equation is

$$K_F = \frac{K_{I,e}}{1 - m\left(\frac{S_n}{S_u}\right)} \qquad \left(S_n \leq \sigma_{ys}\right) \qquad (1)$$

For the surface-crack and corner-crack specimens, S_u is equal to σ_u, the ultimate tensile strength. (For other specimen types, S_u may be greater than σ_u (ref. 6).) The fracture parameters K_F and m are assumed to be constant for a given combination of material thickness, temperature, and rate of loading. To obtain fracture constants that are representative for a given material and test temperature, the nominal failure stress must be less than σ_{ys}, and the fracture data should all be from the same specimen thickness and from tests that encompass a wide range of specimen widths or crack lengths. Reference 4 shows how the fracture parameters are determined from a given set of fracture data.

Equation (1) was derived for $S_n \leq \sigma_{ys}$, but reference 4 has shown that equation (1) closely approximates the failure stresses for surface-cracked specimens even when S_n

4

was greater than σ_{ys}. Therefore, for the present study of surface cracks and corner cracks at holes, equation (1) was also applied for $S_n > \sigma_{ys}$.

ELASTIC STRESS-INTENSITY FACTORS

The form of the elastic stress distribution near a crack tip that contains the stress-intensity factor K_I and the square-root singularity is well known (ref. 2). (The determination of K_I is the basis for linear elastic fracture mechanics.) The stress-intensity factor is a function of load, configuration (specimen type), and the size, shape, and location of the crack. In general, the stress-intensity factor can be expressed as

$$K_{I,e} = S_n \sqrt{\pi c}\ F \tag{2}$$

for any Mode I crack configuration where S_n is the nominal (net section) stress, c is the initial crack length (defined in fig. 1), and F is the boundary correction factor. The boundary correction factor accounts for the influence of various boundaries and crack shapes on stress intensity.

Previous solutions for the elastic stress-intensity factors or the boundary correction factors for a surface crack (refs. 11 to 13) and a corner crack at a hole (refs. 8 to 10 and 14) either were restricted to limited ranges of crack shape and crack size or were presented in graphical form. To eliminate some of the restrictions and for ease of computation, empirical equations which approximate the elastic stress-intensity factors for these crack configurations are developed in the appendix and are compared with other theoretical and experimental stress-intensity factors from the literature. The following sections give the nominal stress equation and the boundary correction factor equation to be used in equation (2) for the surface-crack and corner-crack specimens.

Surface-Crack Specimen

For the surface-crack specimen with a semielliptical crack (fig. 1(a)), the elastic stress-intensity factor at failure is given by equation (2) where the nominal (net section) stress expressed in terms of the gross stress is

$$S_n = \frac{S}{1 - \frac{\pi}{2}\frac{a}{t}\frac{c}{W}} \tag{3}$$

and

$$F = \left(1 - \frac{\pi}{2}\frac{a}{t}\frac{c}{W}\right)\sqrt{\frac{a}{cQ}}\ M_e \tag{4}$$

In equation (4), the term in parentheses converts the gross section stress to the net section stress; the square-root term adjusts the through-crack solution to treat the surface-crack configuration; and M_e is the combined front-face, back-face, and finite-width correction factor (ref. 4). The elastic shape factor Q was given in reference 11 as the square of the elliptic integral of the second kind. An expression was chosen in reference 4 to give a simple approximation and is given by

$$Q = 1 + 1.47\left(\frac{a}{c}\right)^{1.64} \qquad \left(\frac{a}{c} \leq 1.0\right)$$

$$Q = 1 + 1.47\left(\frac{c}{a}\right)^{1.64} \qquad \left(\frac{a}{c} > 1.0\right) \qquad (5)$$

The expression for M_e was developed in reference 4 and is given by

$$M_e = \left[M_1 + \left(\sqrt{Q\frac{c}{a}} - M_1\right)\left(\frac{a}{t}\right)^p\right]f_w \qquad (6)$$

where

$$p = 2 + 8\left(\frac{a}{c}\right)^3 \qquad (7)$$

The term M_1 is the front-face correction, the a/t term is the back-face correction, and f_w is the finite-width correction. The expression for M_1 is given by

$$M_1 = 1.13 - 0.1\frac{a}{c} \qquad \left(0.02 \leq \frac{a}{c} \leq 1.0\right)$$

$$M_1 = \sqrt{\frac{c}{a}}\left(1 + 0.03\frac{c}{a}\right) \qquad \left(\frac{a}{c} > 1.0\right) \qquad (8)$$

and f_w is given by

$$f_w = \sqrt{\sec\left(\frac{\pi c}{W}\sqrt{\frac{a}{t}}\right)} \qquad (9)$$

Corner-Crack Specimens

Uniform stress.- For the corner-crack specimen with a quarter-elliptical crack (fig. 1(b)), the elastic stress-intensity factor is also given by equation (2) where

6

$$S_n = \frac{S}{1 - \dfrac{D}{W} - \dfrac{b\pi}{4} \dfrac{a}{t} \dfrac{c}{W}} \qquad (10)$$

and

$$F = \left(1 - \frac{D}{W} - \frac{b\pi}{4} \frac{a}{t} \frac{c}{W}\right)\sqrt{\frac{a}{cQ}}\, M_e f_b \sqrt{\sec \frac{\pi D}{2W}} \qquad (11)$$

These equations apply for either one (b = 1) or two symmetrical (b = 2) corner cracks. In equation (11), the term in parentheses converts the gross section stress to net section stress; the square-root term containing Q adjusts the through-crack solution to treat the surface-crack configuration; M_e is the combined front-face, back-face, and finite-width correction factor; f_b is the Bowie correction factor (ref. 15) for a through crack (b = 1) or two symmetrical through cracks emanating from a hole (b = 2); and the secant term accounts for the effect of the finite width on stress concentration at the hole.

The value of Q is computed from equation (5) and M_e is given by equation (6). The expression for M_1 in equation (6) is given by

$$M_1 = 1.2 - 0.1 \frac{a}{c} \qquad\qquad \left(0.02 \leq \frac{a}{c} \leq 1.0\right)$$

$$M_1 = \sqrt{\frac{c}{a}}\left(1 + 0.1 \frac{c}{a}\right) \qquad\qquad \left(\frac{a}{c} > 1.0\right) \qquad (12)$$

and f_w is given by

$$f_w = \sqrt{\sec\left(\frac{\pi}{2} \frac{D + bc}{W - 2c + bc} \sqrt{\frac{a}{t}}\right)} \qquad (13)$$

The Bowie correction f_b is given by the following equations (fitted herein to Bowie's numerical results (ref. 15)) for one (b = 1) or two (b = 2) cracks:

$$f_1 = 0.707 - 0.18\lambda + 6.55\lambda^2 - 10.54\lambda^3 + 6.85\lambda^4$$

$$f_2 = 1.0 - 0.15\lambda + 3.46\lambda^2 - 4.47\lambda^3 + 3.52\lambda^4 \qquad (14)$$

where

$$\lambda = \frac{1}{1 + \dfrac{2c}{D}}$$

for all values of c/D. Equations (14) agree within ±2 percent of the numerical values given by Bowie (ref. 15).

Pin loading.- For the pin-loaded corner-crack specimens with a quarter-elliptical crack (fig. 1(c)), the elastic stress-intensity factor is given by equation (2) where

$$S_n = \frac{P}{Wt\left(1 - \frac{D}{W} - \frac{b\pi}{4}\frac{a}{t}\frac{c}{W}\right)} \tag{15}$$

and

$$F = \left(1 - \frac{D}{W} - \frac{b\pi}{4}\frac{a}{t}\frac{c}{W}\right)\sqrt{\frac{a}{cQ}}\, M_e f_b \sqrt{\sec\frac{\pi D}{2W}}\, G_b \tag{16}$$

These equations apply for either one (b = 1) or two symmetrical (b = 2) corner cracks. The terms preceding G_b in equation (16) are identical to those given in equation (11). The term G_b converts the stress-intensity factors for the uniformly stressed corner-crack configuration to those for the pin-loaded specimens as follows:

$$G_1 = \frac{1}{2} + \frac{W}{\pi(D + C)}\sqrt{\frac{D}{D + 2c}} \tag{17}$$

for a single corner crack (b = 1) or

$$G_2 = \frac{1}{2} + \frac{W}{\pi(D + 2c)} \tag{18}$$

for two symmetrical corner cracks (b = 2). The appendix gives the details in developing equations (17) and (18).

ANALYSIS OF FRACTURE DATA

Surface-crack fracture data on 7075-T651 aluminum alloy (ref. 7) for two specimen thicknesses and on Ti-6Al-4V titanium alloy (ref. 7) for a wide range of crack shapes and sizes were analyzed by using equation (1). Also analyzed by using equation (1) were surface-crack and corner-crack fracture data from the literature on 2219-T87 aluminum alloy (refs. 7 and 8), 2024-T3 aluminum alloy (ref. 9), Ti-5Al-2.5Sn (ELI) titanium alloy (ref. 8), and 4340 steel (ref. 10). The fracture parameters K_F and m for a given material, thickness, and test temperature were determined from fracture data for either

8

the surface-crack or the corner-crack configuration. These values of K_F and m were then used to predict the failure stresses for the other crack configuration if data were available for comparison. Failure stress was calculated by substituting equation (2) into equation (1), which gives

$$S_n = \frac{K_F}{\sqrt{\pi c}\ F + \dfrac{mK_F}{S_u}} \tag{19}$$

for $S_n \leq \sigma_{ys}$. Although equation (19) was derived for $S_n \leq \sigma_{ys}$, reference 4 has shown that equation (19) closely approximates the failure stresses for surface-cracked specimens when S_n is greater than σ_{ys}. Therefore, for the present study of surface cracks and corner cracks at holes, equation (19) is also applied for $S_n > \sigma_{ys}$. For extremely small crack sizes, equation (19) predicts nominal failure stresses greater than S_u, but in these cases S_n is set equal to S_u.

<div align="center">Aluminum Alloy Specimens</div>

7075-T651.- Masters, Bixler, and Finger (ref. 7) conducted fracture tests on 7075-T651 aluminum alloy surface-crack specimens for two specimen thicknesses (5 and 13 mm) at room temperature. The tests included a wide variation in crack size ($0.25 \leq a/t \leq 0.95$); the crack shape a/c was about 0.5.

Figure 2 shows the ratio of nominal failure stress S_n to the tensile strength σ_u for the surface-crack tests as a function of cF^2, where c is the crack length and F is the boundary correction factor for the surface crack (eq. (4)). This type of plot (S_n/S_u against cF^2) gives a single curve defined by K_F and m for all crack shapes and crack sizes. The fracture parameters K_F and m for each specimen thickness were determined by a best fit of equation (19) to these data. (The best-fit procedure used is given in ref. 4.) The thicker material exhibited a fracture behavior very similar to that predicted by LEFM (m was nearly zero). The thinner material exhibited higher failure stresses for a given crack size and had larger values of K_F and m than the thicker material. The solid and dashed curves were calculated from the TPFC (eq. (19)) by using the values of K_F and m indicated.

2219-T87.- Masters, Bixler, and Finger (ref. 7) conducted fracture tests on 2219-T87 aluminum alloy surface-crack specimens for several thicknesses at a temperature of 77 K. Hall and Finger (ref. 8) tested both surface-crack and corner-crack specimens (remote uniform stress) made from a different heat of the same alloy and tested at the same temperature. The results from the surface-crack tests were used to obtain the fracture parameters and a comparison was then made between the predicted and experi-

mental failure stresses for the corner-crack tests. Figure 3 shows S_n / σ_u for the surface-crack tests (refs. 7 and 8) (denoted by the symbols) as a function of cF^2. The surface-crack tests for the 5- and 13-mm-thick specimens included a wide variation in crack shape ($0.2 \leq a/c \leq 0.8$) and crack size ($0.25 \leq a/t \leq 0.9$). The 18-mm-thick specimens had a value of a/t of about 0.5, with a/c equal to either 0.2 or 0.5. The fracture parameters K_F and m were determined by a best fit of equation (19) to these data. The failure stresses calculated from the TPFC (eq. (19)) for each thickness are shown by the curves. The experimental failure stresses generally were within ±10 percent of the calculated failure stresses.

The corner-crack tests conducted by Hall and Finger (ref. 8) on the same alloy and tested at the same temperature as the 18-mm-thick surface-crack specimens are shown in figure 4. The corner-crack tests included variations in the hole diameter-thickness ratio (D/t = 0.5 and 1.0), crack shape ($0.2 \leq a/c \leq 1.1$), and crack size ($0.2 \leq a/t \leq 0.8$). Figure 4 shows the ratio of nominal failure stress S_n to the tensile strength σ_u for the corner-crack data as a function of cF^2, where c is the crack length from the hole and F is the boundary correction factor for the corner crack (eq. (11)). The fracture parameters K_F and m, determined from the surface-crack tests, were also assumed to apply for the corner-crack tests. The experimental failure stresses (open symbols) generally were within ±10 percent of the predicted results (dashed curve). The solid curve shows the results of a best fit of equation (19) to the corner-crack data. The fracture parameters obtained from the corner-crack data were slightly lower than those obtained from the surface-crack data. The fracture parameters obtained from the corner-crack data are considered to be more representative for this material and test temperature. The results of the four surface-crack tests (denoted by the × symbol) are also shown in figure 4 for reference. These results demonstrate how well the TPFC correlated fracture data from surface-crack and corner-crack specimens for a wide range of crack shape a/c and crack size a/t.

2024-T3.- Broek, Nederveen, and Meulman (ref. 9) conducted surface-crack and corner-crack fracture tests on 2024-T3 aluminum alloy sheet and plate material at room temperature. The four material thicknesses ranged from 5 to 35 mm. For the surface cracks, a/t varied from 0.6 to 1.0 and a/c was near unity. For the corner cracks, a/t varied from 0.5 to 1.0 and a/c was again near unity. Because 2024-T3 aluminum alloy material does not exhibit a strong thickness effect (ref. 16), fracture data for all thicknesses tested in reference 9 were analyzed as one group. The results from the surface-crack tests were used to obtain the two fracture parameters. A comparison was then made between the predicted and experimental failure stresses for the corner-crack tests.

Figure 5 shows the surface-crack fracture data (ref. 9) for the 2024-T3 aluminum alloy material. The fracture parameters $\left(K_F = 132 \text{ MN}/\text{m}^{3/2} \text{ and } m = 1.0 \right)$ were

10

obtained by a best fit of equation (19) to these data (solid curve). A value of 1 for the fracture-toughness parameter m indicated that the material was very ductile, and the failure stresses were nearly equal to the yield stress of the material (dashed line). The experimental failure stresses (symbols) fell within ±10 percent of the calculated results (solid curve). Figure 6 shows the corner-crack fracture data for both uniformly stressed specimens (open symbols) and pin-loaded specimens (solid symbols). Again, the fracture parameters K_F and m, determined from the surface-crack tests, were assumed to apply for corner cracks. The solid curve shows the predictions from equation (19). The experimental data were within ±10 percent of the predicted results, even though the hole diameter was 40 percent of the specimen width and some of the corner cracks had cracked areas as large as 30 percent of the net section area.

Titanium Alloy Specimens

Ti-6Al-4V.- Masters, Bixler, and Finger (ref. 7) conducted fracture tests on surface-crack specimens made of Ti-6Al-4V titanium alloy at room temperature. The tests included variations in crack shape ($0.2 \leq a/c \leq 0.8$) and crack size ($0.3 \leq a/t \leq 0.9$). The results are shown in figure 7. The fracture parameters K_F and m were determined by a best fit of equation (19) to these data. The solid curve shows the calculations from the TPFC. The experimental failure stresses (symbols) were within ±13 percent of the calculated failure stresses.

Ti-5Al-2.5Sn.- Hall and Finger (ref. 8) tested both surface-crack and corner-crack specimens made of Ti-5Al-2.5Sn (ELI) titanium alloy at a temperature of 77 K. The surface-crack tests had a value of a/t of about 0.4 and a value of a/c of about 0.6. The corner-crack tests included variations in hole diameter-thickness ratio ($D/t = 0.5$ and 1.0), crack shape ($0.2 \leq a/c \leq 1.1$), and crack size ($0.2 \leq a/t \leq 0.8$).

Figure 8 shows the surface-crack and corner-crack fracture data (symbols) for this titanium alloy. The fracture parameters $\left(K_F = 82.9 \text{ MN}/\text{m}^{3/2} \text{ and } m = 0.08\right)$ were determined by a best fit of equation (19) to only the corner-crack data. (The fracture parameters could not be determined from the surface-crack data because all tests were conducted with the same crack size and shape.) The experimental failure stresses generally were within ±15 percent of the calculated results (solid curve). The solid curve also shows the predicted results for the surface-crack tests (denoted by the × symbol).

4340 Steel Specimens

Hall, Shah, and Engstrom (ref. 10) conducted fracture tests on high-strength 4340 steel surface-crack and corner-crack specimens at room temperature. The corner-crack specimens (remote uniform stress) had either one or two (symmetrical) corner cracks at the edge of the hole. The corner-crack tests included variations in hole diameter-

thickness ratio (D/t = 0.83 and 1.25) and crack size (0.4 ≤ a/t ≤ 0.8), but the crack shape a/c was approximately unity. The fracture parameters K_F and m were determined from the corner-crack fracture data (shown as open and solid symbols in fig. 9). The best fit of equation (19) to the corner-crack fracture data required that m be negative (m = -0.9), which is in violation of the bounds imposed on m in the derivation of equation (1). In reference 4, a negative value of m also occurred for a few surface-crack fracture specimens made of low-toughness materials and was attributed in reference 4 to a compressive residual stress near the surface of the plate. Because the stress-intensity factor used in equation (1) did not include the contribution from the residual stresses, the parameter m adjusted itself to account for this deficiency, which resulted in a negative value. Elber (ref. 17) has shown that residual stresses near the surface of a plate can significantly affect the failure stresses for surface-cracked specimens and that the contribution of the residual stresses to the stress-intensity factor should be included. The presence or absence of residual stresses in these specimens was not established in reference 10. However, the material, being of high strength, was difficult to machine, and therefore, the specimens are suspected of having high residual machining stresses.

The surface-crack and corner-crack results (symbols) for the 4340 steel are shown in figure 9. The solid curve was calculated from equation (19) by using $K_F = 50.5$ $MN/m^{3/2}$ and $m = -0.9$. The dashed curve shows the calculations from equation (19) with $K_F = 69.6$ $MN/m^{3/2}$ and $m = 0$ (LEFM). This high-strength steel should exhibit a very brittle fracture behavior (ref. 10). The corner-crack failure stresses were within ±10 percent of the calculated results (solid or dashed curve); additional tests at smaller crack lengths would be required to establish the correct behavior in that range. The two surface-crack results were higher (about 15 percent) than the predicted results (solid or dashed curve). For this material, the differences between the surface-crack and corner-crack results could stem from either the approximate nature of the boundary correction factors for these cracked configurations or the residual stresses. The effects of residual stresses should be considered whenever surface-crack or corner-crack specimens are being made, especially for high-strength materials. The effects of residual stresses on fracture toughness need to be studied further.

CONCLUDING REMARKS

An equation that relates the elastic stress-intensity factor at failure, the elastic nominal failure stress, and two material fracture parameters has been applied as a two-parameter fracture criterion (TPFC) to fracture data reported in the literature for surface cracks and corner cracks (surface cracks at the edge of a hole) in specimens of aluminum alloy, titanium alloy, and steel. The surface-crack specimens were subjected to remote uniform stress, whereas the corner-crack specimens were subjected to either

remote uniform stress or pin loading in the hole. The corner-crack specimens had either one or two (symmetrical) surface cracks emanating from the hole. Wide ranges of crack shape (ratios of crack depth to crack length from 0.2 to 1.1) and crack size (ratios of crack depth to specimen thickness from 0.2 to 1.0) were considered. The TPFC correlated and predicted failure stresses for surface-cracked and corner-cracked specimens within ±10 percent for most of the data analyzed.

Stress-intensity-factor equations used in the TPFC for the corner crack (or cracks) emanating from a circular hole in a finite-thickness and finite-width specimen were developed. These equations are compared in the appendix with experimental (photoelastic) stress-intensity factors from the literature and agree generally within ±10 percent of the average of the experimental stress-intensity factors along the crack front. As the crack depth approaches the specimen thickness, the stress-intensity factors calculated from these equations approached (within ±2 percent) the theoretical stress-intensity factors for a through crack.

Langley Research Center
National Aeronautics and Space Administration
Hampton, Va. 23665
May 10, 1976

APPENDIX

DEVELOPMENT OF STRESS-INTENSITY FACTORS FOR SURFACE CRACKS
AND CORNER CRACKS AT HOLES IN FINITE PLATES

Several investigators have obtained approximate stress-intensity factors for surface cracks and corner cracks at holes in infinitely wide plates. In this section, empirical stress-intensity factor equations are presented for surface cracks (ref. 4) and developed for corner cracks at holes for a wide range of crack shapes a/c and crack sizes a/t in finite-thickness and finite-width specimens. Because of the similarity between the surface-crack and corner-crack configurations, the stress-intensity factors from the surface crack were used to help establish those for the corner crack. These equations are compared with other theoretical and experimental (photoelastic) stress-intensity factors from the literature.

Surface Crack

Background.- Irwin (ref. 11) derived an expression for the stress-intensity factor around an elliptical crack in an infinite elastic solid subjected to uniaxial tension. The stress-intensity factor along the boundary of the elliptical crack in an infinite solid, subjected to a remote uniaxial stress S acting normal to the plane of the crack, is given by

$$K_I = S\sqrt{\frac{\pi a}{Q}}\left(\frac{a^2}{c^2}\cos^2\theta + \sin^2\theta\right)^{1/4} \tag{A1}$$

For $c \geqq a$, the maximum stress-intensity factor is given by

$$K_I = S\sqrt{\frac{\pi a}{Q}} \tag{A2}$$

Irwin (ref. 11) also estimated the stress-intensity factor for a semielliptical crack in a finite-thickness infinitely wide specimen. (See fig. 1(a) for $W \gg c$.) His equation was restricted to crack depths less than one-half the plate thickness.

The boundary correction factors for a surface crack in an infinitely wide plate as a function of a/t and a/c were obtained from the analytical results of references 12, 13, and 18. Smith and Alavi (ref. 12) obtained approximate solutions for a near penny-shaped crack ($a/c = 0.4$ and 1.0) as a function of a/t. For shallow cracks, Rice and Levy (ref. 13) obtained approximate solutions for $a/c = 0.1$ and 0.2 as a function of a/t. Gross and Srawley (ref. 18) obtained a solution for $a/c = 0$ (an edge-cracked plate).

14

APPENDIX

Finite plate subjected to uniform stress.- In reference 4, an expression for the boundary correction factor on stress intensity for a surface crack in a finite-thickness specimen was obtained by fitting an empirical equation to the analytical results from references (refs. 12, 13, and 18). The equation was chosen so that the stress-intensity factor for a through crack in a finite-width specimen (ref. 1) was obtained when the surface crack intersects the back surface of the plate (a = t). The elastic stress-intensity factor for the configuration shown in figure 1(a) is given by

$$K_I = S\sqrt{\pi \frac{a}{Q}} \, M_e \tag{A3}$$

The elastic shape factor Q was given in reference 11 as the square of the elliptic integral of the second kind. An expression was chosen in reference 4 to give a simple approximation and is given by

$$Q = 1 + 1.47\left(\frac{a}{c}\right)^{1.64} \qquad \left(\frac{a}{c} \leq 1.0\right)$$

$$Q = 1 + 1.47\left(\frac{c}{a}\right)^{1.64} \qquad \left(\frac{a}{c} > 1.0\right) \tag{A4}$$

The maximum error in the stress-intensity factor using these approximate equations for Q is less than 0.25 percent. The boundary correction factor M_e developed in reference 4 is given by

$$M_e = \left[M_1 + \left(\sqrt{Q \frac{c}{a}} - M_1\right)\left(\frac{a}{t}\right)^p\right] f_w \tag{A5}$$

where

$$p = 2 + 8\left(\frac{a}{c}\right)^3 \tag{A6}$$

M_1 is the front-face correction, and the a/t term is the back-face correction. The expression for M_1 is given by

$$M_1 = 1.13 - 0.1\frac{a}{c} \qquad \left(0.02 \leq \frac{a}{c} \leq 1.0\right)$$

$$M_1 = \sqrt{\frac{c}{a}}\left(1 + 0.03\frac{c}{a}\right) \qquad \left(\frac{a}{c} > 1.0\right) \tag{A7}$$

15

APPENDIX

The term f_W accounts for the influence of the finite width and is given by

$$f_W = \sqrt{\sec\left(\frac{\pi c}{W} \sqrt{\frac{a}{t}}\right)} \qquad\qquad (A8)$$

The equation for f_W proposed herein is slightly different from the original equation proposed for f_W in reference 4. The new equation was chosen because Jolles, McGowan, and Smith (ref. 19) have experimentally shown that the original equation slightly underestimated the influence of specimen width on stress intensity (less than 7 percent) for a large surface crack ($2c/W = 0.81$, $a/t = 0.36$, $a/c = 0.07$) in a finite-thickness and finite-width specimen. The new equation is in better agreement with the experimental stress-intensity factors.

The equation for the boundary correction factor (eq. (A5)) is an approximate equation which accounts for the influence of the front face, back face, and finite width on stress intensity. Figure 10 shows calculations from equation (A5) divided by the square root of Q (solid curves) as a function of a/c and a/t for $W = \infty$ (or $f_W = 1$). The correction factors given by equation (A5) agree fairly well with the analytical results of references 12, 13, and 18. For $a/c > 1.0$, the maximum stress-intensity factor is near $\theta = 0$ and π (see the insert in fig. 10), and the correction factors are not influenced strongly by a/t.

Equation (A5) was compared with experimental (photoelastic) stress-intensity factors in reference 20 and generally agreed to within ±10 percent of the experimental values. Although equation (A5) gives only a single value of stress intensity for each configuration (independent of the angle θ), this value of stress intensity is assumed, as in reference 4, to occur at the location along the crack front at which fracture initiates.

As a/t approaches unity for any value of a/c (except zero), equation (A3) reduces to the stress-intensity factor for a through crack of length $2c$ in a finite-width plate (ref. 1), which is given by

$$K_I = S\sqrt{\pi c \sec \frac{\pi c}{W}} \qquad\qquad (A9)$$

Corner Cracks at Holes

Background.- Several investigators (refs. 8 to 10 and 14) have obtained approximate stress-intensity factors for the corner crack (or cracks) at the edge of a circular hole. These approximations had some limitations on crack shape a/c or crack size a/t. Other investigators (refs. 21 and 22) have obtained experimental (photoelastic) stress-intensity factors for a corner crack at a hole in a finite plate.

16

APPENDIX

In the present paper, empirical stress-intensity-factor equations are developed for a corner crack (or cracks) emanating from a circular hole in a finite plate subjected to either remote uniform stress or pin loading in the hole for a wide range of crack shape a/c and size a/t. These equations are compared with other theoretical and experimental stress-intensity factors from the literature.

Finite plate subjected to uniform stress.- The stress-intensity factor for either one or two (symmetrical) corner cracks emanating from a circular hole in a finite-thickness and finite-width specimen subjected to remote uniform stress (fig. 1(b)) is given by

$$K_I = S\sqrt{\pi \frac{a}{Q}}\ M_e f_b \sqrt{\sec \frac{\pi D}{2W}} \tag{A10}$$

where $b = 1$ for a single corner crack and $b = 2$ for two symmetrical corner cracks. The equation for Q is given by equation (A4) and M_e is given by equation (A5). The term M_1 in equation (A5) is given by

$$M_1 = 1.2 - 0.1 \frac{a}{c} \qquad \left(0.02 \leq \frac{a}{c} \leq 1.0\right)$$
$$\left.\begin{array}{l} \\ \\ M_1 = \sqrt{\frac{c}{a}}\left(1 + 0.1 \frac{c}{a}\right) \qquad \left(\frac{a}{c} > 1.0\right)\end{array}\right\} \tag{A11}$$

These equations are similar to equations (A7) except that they account for an interaction between the hole and the front face. These equations were chosen so that the stress-intensity factors for $W = \infty$ would approach the correct limiting values as a/c becomes large or as the hole radius becomes large with $a/c = 1$ or infinity. The finite-width correction is given by

$$f_w = \sqrt{\sec\left(\frac{\pi}{2} \frac{D + bc}{W - 2c + bc} \sqrt{\frac{a}{t}}\right)} \tag{A12}$$

This equation for f_w was chosen to approximately account for the effects of crack eccentricity on stress intensity (ref. 23) for a single crack ($b = 1$) emanating from a hole. Equation (A12) also reduces to equation (A8) for $b = 2$ and $D = 0$.

The term f_b in equation (A10) is the Bowie correction for a through crack (or cracks) emanating from a circular hole (eq. (14)), and the secant term in equation (A10) accounts for an interaction between the hole and the finite width (see ref. 24, p. 42).

Figure 11 shows the stress-intensity factors from equation (A10) normalized by $K_{I,b}$ (Bowie's stress-intensity factor for a through crack of length c emanating from

17

a circular hole) as a function of a/t and a/c for D/t = 1 and W = ∞. As a/t approaches unity or a/c approaches infinity, the stress intensity K_I approaches $K_{I,b}$. Although equation (A10) gives only a single value of stress intensity for each configuration, independent of the angle θ (see the insert in fig. 9), this value of stress intensity is assumed to occur at the location along the crack front at which fracture initiates.

Figures 12 and 13 show a comparison between the theoretical stress-intensity factors from Hall and Finger (ref. 8), Shah (ref. 14), and from equation (A10) for a/c = 1.0 and 0.25, respectively. All stress intensities are normalized by $K_{I,b}$ with D/t = 1 and W = ∞ (or f_w = 1). At small values of a/t, Shah's results are in good agreement with equation (A10) for both values of a/c. (Shah had selected θ = 65° as the location at which fracture initiates.) For a/c = 0.25, Shah's results are also in good agreement (±10 percent) with equation (A10) for all values of a/t. However, the Hall and Finger results are generally 10 to 30 percent higher than equation (A10) for both values of a/c.

Figure 14 shows a comparison between the experimental (photoelastic) (refs. 21 and 22) and the calculated (eq. (A10)) stress-intensity factors normalized by $K_{I,b}$ for 14 different corner-cracked configurations (symbols). A wide range of crack shapes and crack sizes was considered. The experimental stress-intensity factor was the average of two stress intensities obtained from different locations along the crack front. One location was at the intersection of the crack front with the plate surface (see the insert in the figure) with the stress intensity denoted by $K_{I,s}$, and the other location was at the hole surface with stress intensity denoted by $K_{I,h}$. The stress-intensity factors calculated from equation (A10) generally were within ±10 percent of the average of $K_{I,s}$ and $K_{I,h}$.

As a/t approaches unity for any value of a/c (except zero), equation (A10) reduces to the equation for the stress-intensity factor for a through crack (or cracks) emanating from a circular hole in a finite-width plate and is given by

$$K_I = S\sqrt{\pi c}\ f_w f_b \sqrt{\sec \frac{\pi D}{2W}} \tag{A13}$$

where f_w is given by equation (A12) with a/t = 1 and f_b is given by equation (14). Equation (A13) gives stress-intensity factors within ±2 percent of the values calculated by Newman (ref. 24) using boundary collocation for two symmetrical through cracks emanating from a circular hole in a finite-width plate.

Finite plate subjected to pin loading.- The stress-intensity factors for either one or two cracks emanating from a circular hole subjected to pin loading in the hole were obtained by superposition of known solutions for stress intensity (similar to that given in ref. 9). For example, a crack emanating from a pin-loaded hole is similar to the wedge-force-loaded crack (ref. 23). Figure 15 shows how the stress-intensity factor $K_{I,sp}$ at

18

point A for the wedge-force-loaded through crack (supported by uniform stress at one end) was obtained by superposition of known solutions. The stress intensity for the uniformly stressed plate is

$$K_{I,ss} = S\sqrt{\pi c'} f_w \tag{A14}$$

and for the wedge-force-loaded crack at point A (ref. 22) is

$$K_{I,pp} = \frac{P}{t\sqrt{\pi c'}} \sqrt{\frac{c' - x}{c' + x}} f_w \tag{A15}$$

The finite-width correction f_w for the uniformly stressed plate was also assumed to apply for the wedge-force-loaded plate. The stress intensity $K_{I,sp}$ is given by

$$K_{I,sp} = K_{I,ss} + K_{I,pp} - K_{I,sp} \tag{A16}$$

or

$$K_{I,sp} = \frac{1}{2}\left(K_{I,ss} + K_{I,pp}\right) \tag{A17}$$

Substituting equations (A14) and (A15) into equation (A17) gives

$$K_{I,sp} = K_{I,ss}\left(\frac{1}{2} + \frac{W}{2\pi c'}\sqrt{\frac{c' - x}{c' + x}}\right) = K_{I,ss}G \tag{A18}$$

where the pin load P was expressed in terms of the uniform stress $(P = SWt)$. Thus, the term in the parentheses, denoted as G, converts the stress-intensity factor for the uniformly stressed plate to that for the wedge-force-loaded plate. The function G was used to convert the stress intensity for the corner-crack specimen under uniform stress to that for pin loading.

The stress-intensity factor for one or two (symmetrical) corner cracks emanating from a circular hole in a finite plate subjected to pin loading in the hole (see fig. 1(c)) was obtained from equation (A18) by replacing $K_{I,ss}$ with equation (A10) and is given by

$$K_I = S\sqrt{\pi\frac{a}{Q}} M_e f_b \sqrt{\sec\frac{\pi D}{2W}} G_b \tag{A19}$$

where

$$G_1 = \frac{1}{2} + \frac{W}{\pi(D + c)} \sqrt{\frac{D}{D + 2c}} \qquad (A20)$$

for a single corner crack (b = 1) and

$$G_2 = \frac{1}{2} + \frac{W}{\pi(D + 2c)} \qquad (A21)$$

for two symmetrical corner cracks (b = 2). Note that c' and x in equation (A18) have been rewritten in terms of the hole diameter D and the crack length from the hole c as $2c' = D + bc$ and $2x = (2 - b)c$. The pin load was assumed to apply at the center line of the hole.

REFERENCES

1. Brown, William F., Jr.; and Srawley, John E.: Plane Strain Crack Toughness Testing of High Strength Metallic Materials. ASTM Spec. Tech. Publ. No. 410, c.1966.

2. Srawley, John E.; and Brown, William F., Jr.: Fracture Toughness Testing Methods. Fracture Toughness Testing and Its Applications, Spec. Tech. Publ. No. 381, Amer. Soc. Testing & Mater., c.1965, pp. 133-198.

3. Kuhn, Paul: Residual Tensile Strength in the Presence of Through Cracks or Surface Cracks. NASA TN D-5432, 1970.

4. Newman, J. C., Jr.: Fracture Analysis of Surface- and Through-Cracked Sheets and Plates. Eng. Fract. Mech., vol. 5, no. 3, Sept. 1973, pp. 667-689.

5. Newman, J. C., Jr.: Plane-Stress Fracture of Compact and Notch-Bend Specimens. NASA TM X-71926, 1974.

6. Newman, J. C., Jr.: Fracture Analysis of Various Cracked Configurations in Sheet and Plate Materials. NASA TM X-72709, 1975.

7. Masters, J. N.; Bixler, W. D.; and Finger, R. W.: Fracture Characteristics of Structural Aerospace Alloys Containing Deep Surface Flaws. NASA CR-134587, 1973.

8. Hall, L. R.; and Finger, R. W.: Fracture and Fatigue Growth of Partially Embedded Flaws. Proceedings of the Air Force Conference on Fatigue and Fracture of Aircraft Structures and Materials, H. A. Wood, R. M. Bader, W. J. Trapp, R. F. Hoener, and R. C. Donat, eds., AFFDL-TR-70-144, U.S. Air Force, Dec. 1970, pp. 235-262.

9. Broek, D.; Nederveen, A.; and Meulman, A.: Applicability of Fracture Toughness Data to Surface Flaws and to Corner Cracks at Holes. NLR TR 71033 U, Nat. Lucht- Ruimtevaartlab. (Amsterdam), Jan. 1971.

10. Hall, L. R.; Shah, R. C.; and Engstrom, W. L.: Fracture and Fatigue Crack Growth Behavior of Surface Flaws and Flaws Originating at Fastener Holes. Volume I — Results and Discussion. AFFDL-TR-74-47, Vol. I, U.S. Air Force, May 1974.

11. Irwin, G. R.: Crack-Extension Force for a Part-Through Crack in a Plate. Trans. ASME, Ser. E: J. Appl. Mech., vol. 29, no. 4, Dec. 1962, pp. 651-654.

12. Smith, F. W.; and Alavi, M. J.: Stress Intensity Factors for a Penny Shaped Crack in a Half Space. Eng. Frac. Mech., vol. 3, no. 3, Oct. 1971, pp. 241-254.

13. Rice, J. R.; and Levy, N.: The Part-Through Surface Crack in an Elastic Plate. Paper No. 71-APM-20, American Soc. Mech. Eng., 1971.

14. Shah, R. C.: Stress Intensity Factors for Through and Part-Through Cracks Originating at Fastener Holes. Mechanics of Crack Growth, ASTM Spec. Tech. Publ. 590, c.1976, pp. 429-459.

15. Bowie, O. L.: Analysis of an Infinite Plate Containing Radial Cracks Orginating at the Boundary of an Internal Circular Hole. J. Math. & Phys., vol. XXXV, no. 1, Apr. 1956, pp. 60-71.

16. Feddersen, C. E.; Simonen, F. A.; Hulbert, L. E.; and Hyler, W. S.: An Experimental and Theoretical Investigation of Plane-Stress Fracture of 2024-T351 Aluminum Alloy. NASA CR-1678, 1970.

17. Elber, Wolf: Effects of Shot-Peening Residual Stresses on the Fracture and Crack-Growth Properties of D6AC Steel. Fracture Toughness and Slow-Stable Cracking, Spec. Tech. Publ. 559, American Soc. Testing & Mater., 1974, pp. 45-58.

18. Gross, Bernard; and Srawley, John E.: Stress-Intensity Factors for Single-Edge-Notch Specimens in Bending or Combined Bending and Tension by Boundary Collocation of a Stress Function. NASA TN D-2603, 1965.

19. Jolles, M.; McGowan, J. J.; and Smith, C. W.: Experimental Determination of Side Boundary Effects on Stress Intensity Factors in Surface Flaws. VPI-E-74-5 (Contract No. DAA-F07-69-C-0444), Virginia Polytech. Inst. & State Univ., Mar. 1974.

20. Harms, A. E.; and Smith, C. W.: Stress Intensity Factors for Long, Deep Surface Flaws in Plates Under Extensional Fields. VPI-E-73-6 (Contract No. NGR 47-004-076), Virginia Polytech. Inst. & State Univ., Feb. 1973. (Available as NASA CR-132015.)

21. McGowan, J. J.; and Smith, C. W.: Stress Intensity Factors for Deep Cracks Emanating From the Corner Formed by a Hole Intersecting a Plate Surface. VPI-E-74-1 (Grant No. NGR 47-004-476), Virginia Polytech. Inst. & State Univ., Jan. 1974. (Available as NASA CR-136930.)

22. Jolles, M.; McGowan, J. J.; and Smith, C. W.: Stress Intensities for Cracks Emanating From Holes in Finite Thickness Plates. VPI-E-75-15 (Grant No. NSG 1024), Virginia Ploytech. Inst. & State Univ., Aug. 1975. (Available as NASA CR-143526.)

23. Tada, Hiroshi; Paris, Paul C.; and Irwin, George R.: The Stress Analysis of Cracks Handbook. Del Research Corp., c.1973.

24. Newman, J. C., Jr.: An Improved Method of Collocation for the Stress Analysis of Cracked Plates With Various Shaped Boundaries. NASA TN D-6376, 1971.
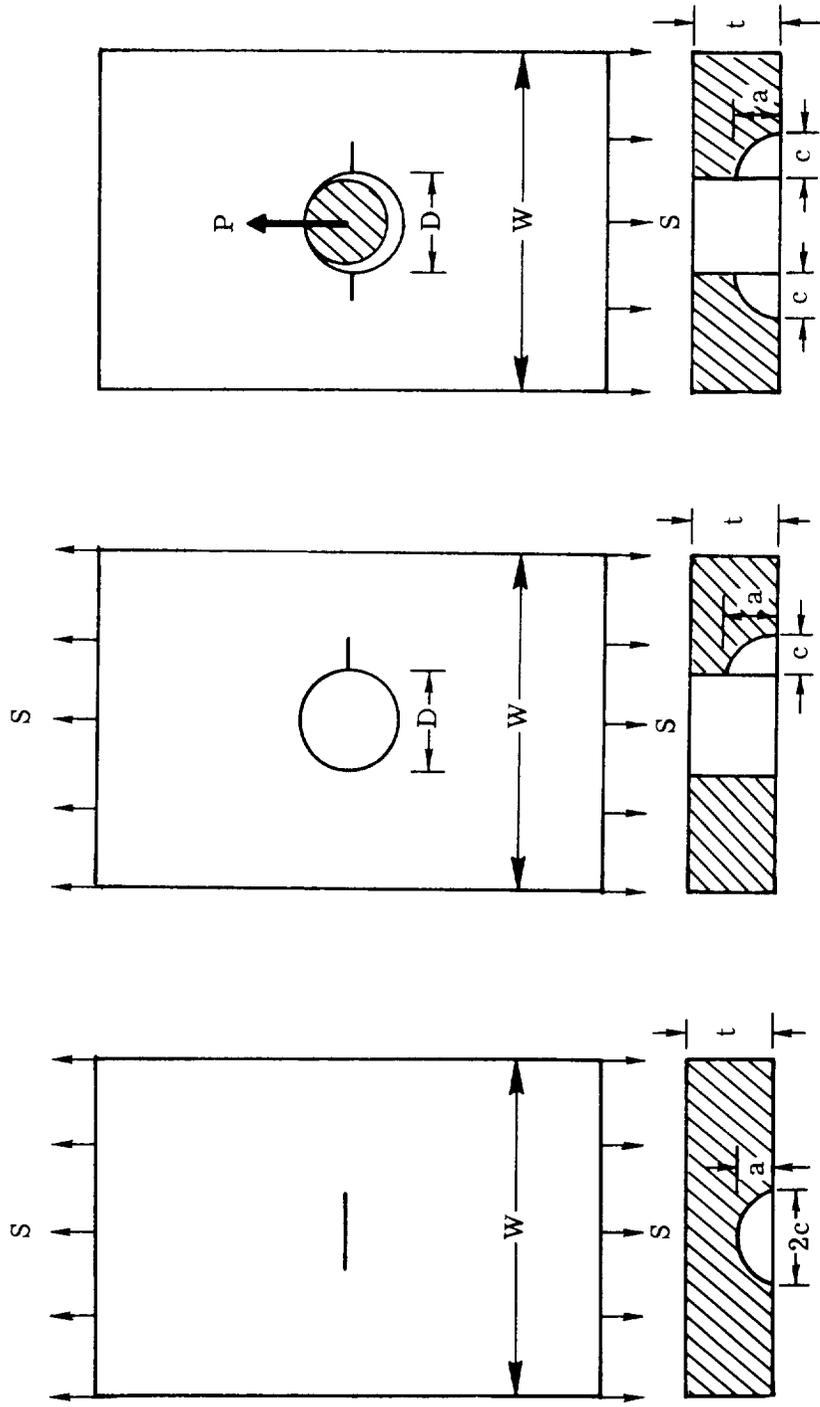
(a) Surface crack.

(b) Corner crack (uniform stress).

(c) Corner crack (pin load).
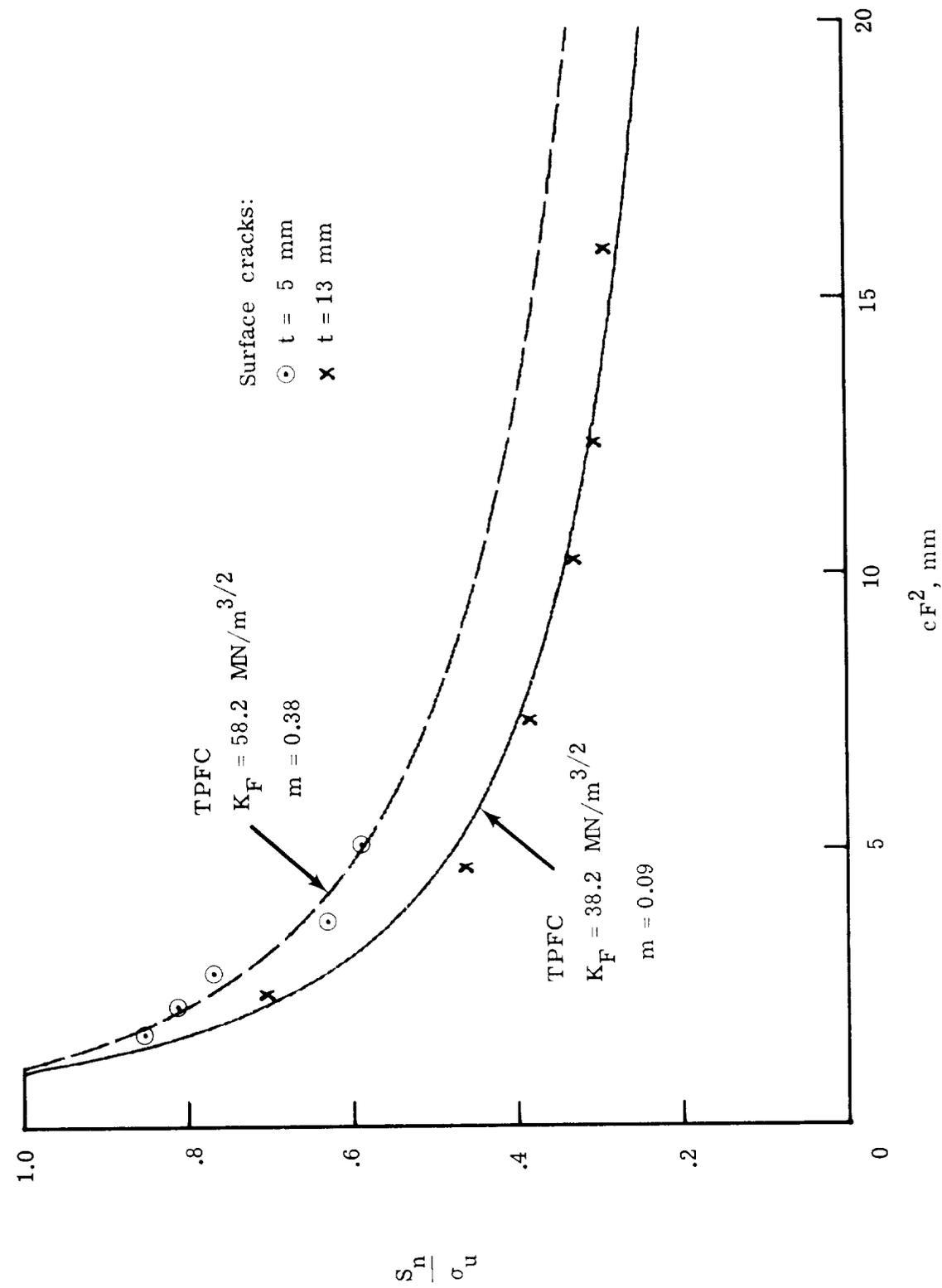
Figure 1.- Surface-crack and corner-crack specimens.

23

Figure 2.- Calculated and experimental surface-crack fracture data for 7075-T651 aluminum alloy (ref. 7). $\sigma_{ys} = 550$ MPa; $\sigma_u = 610$ MPa; room temperature.
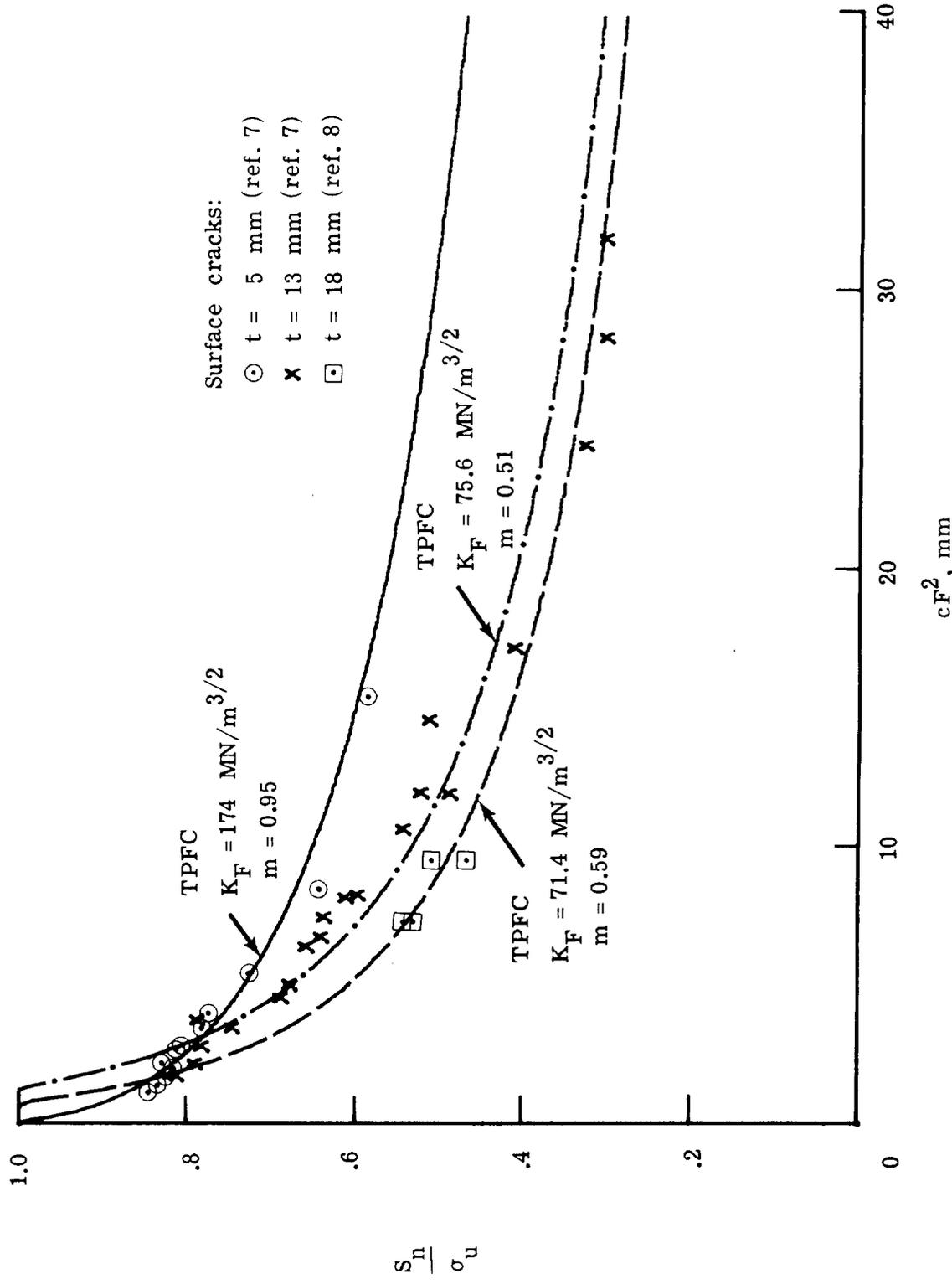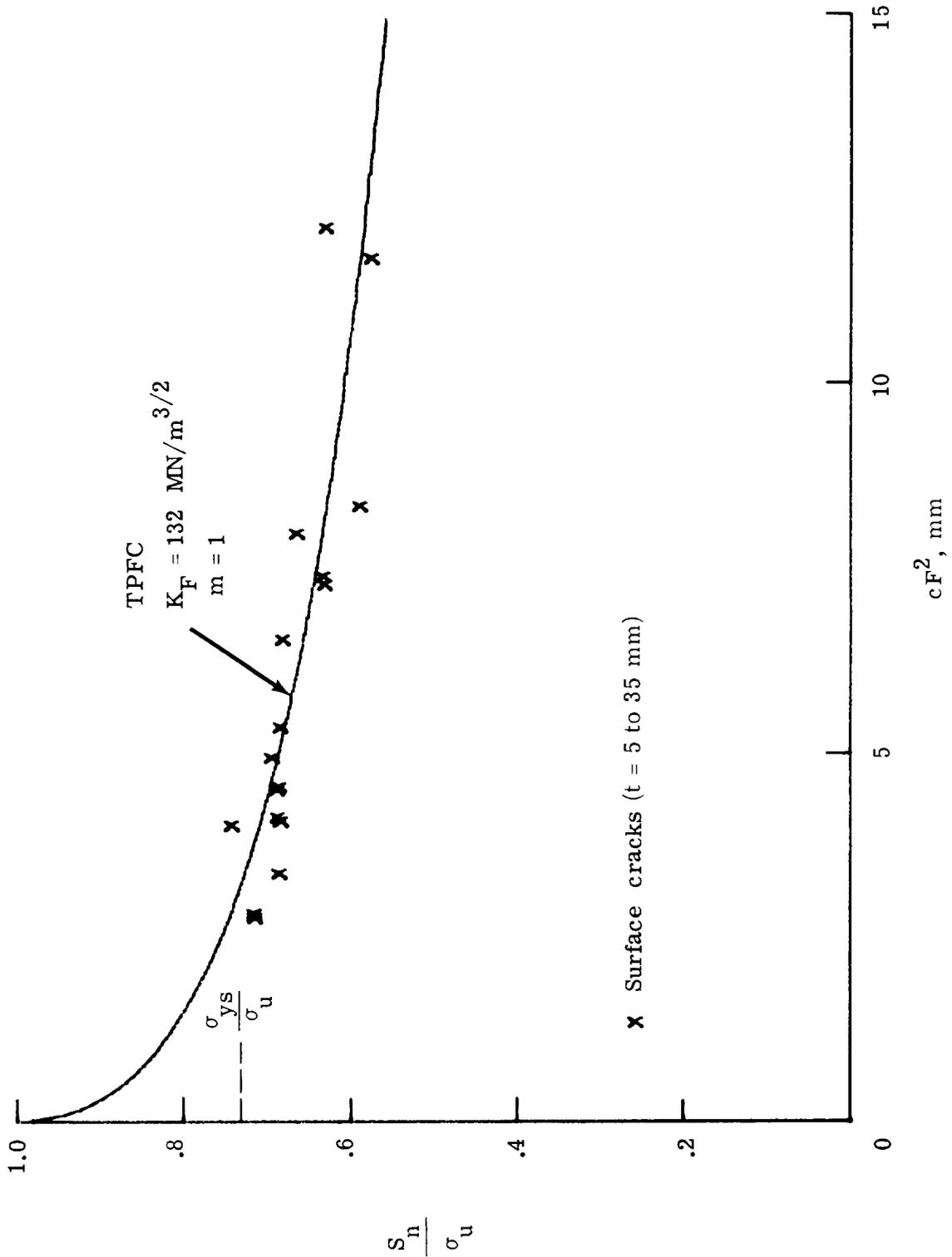
24

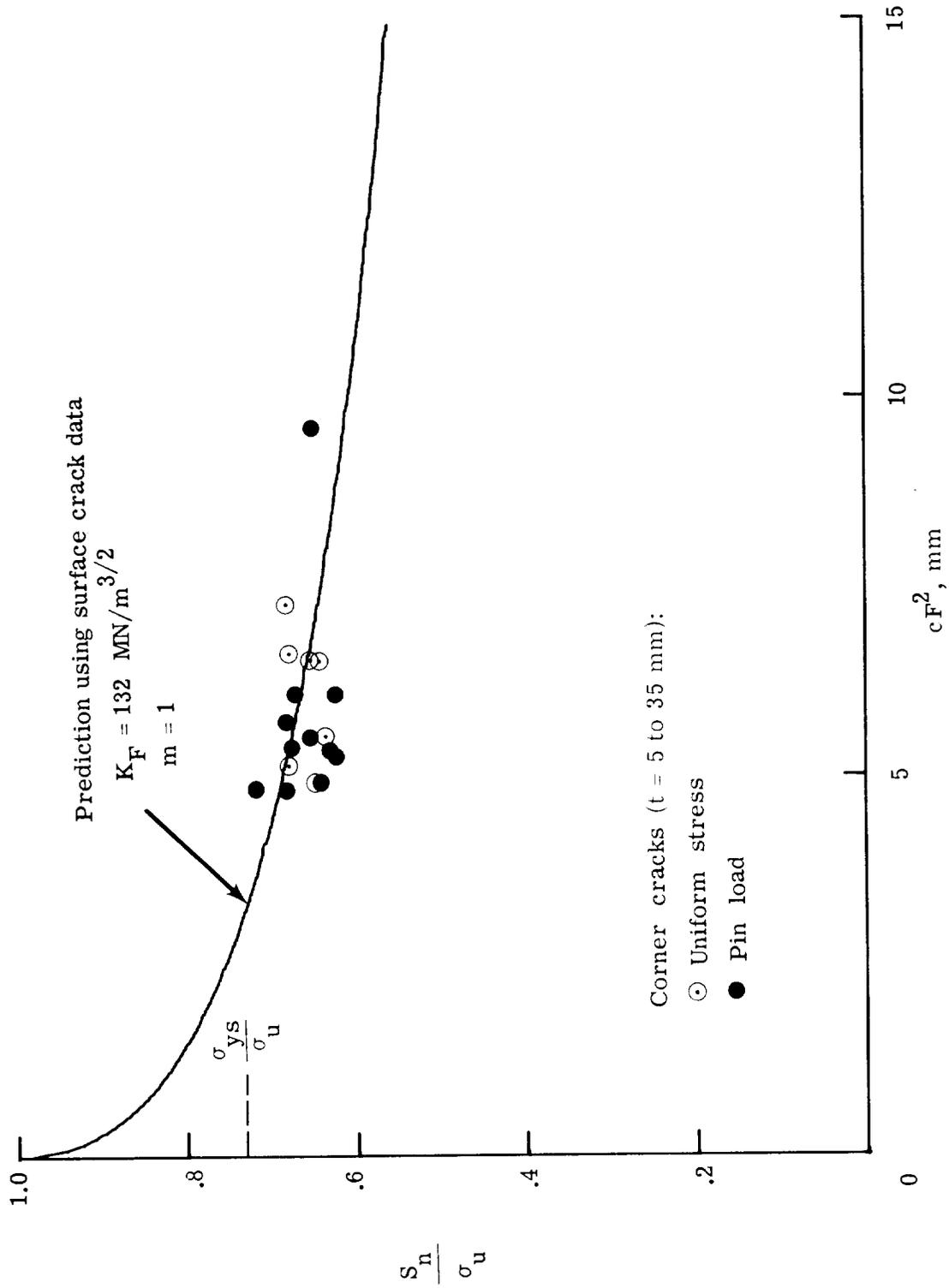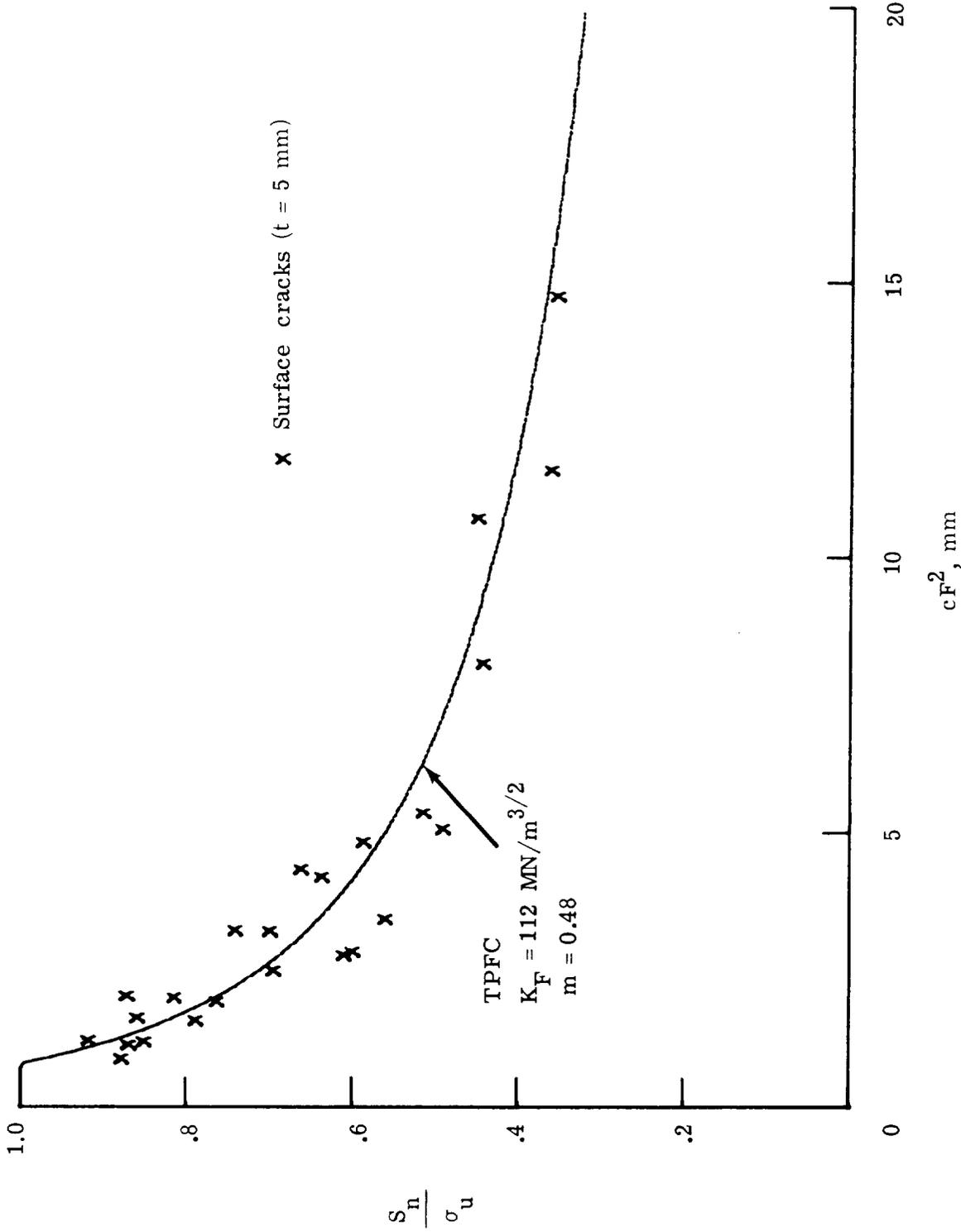Figure 3.- Calculated and experimental surface-crack fracture data for 2219-T87 aluminum alloy (refs. 7 and 8).

$\sigma_{ys} = 455$ MPa; $\sigma_u = 600$ MPa; $T = 77$ K.

25
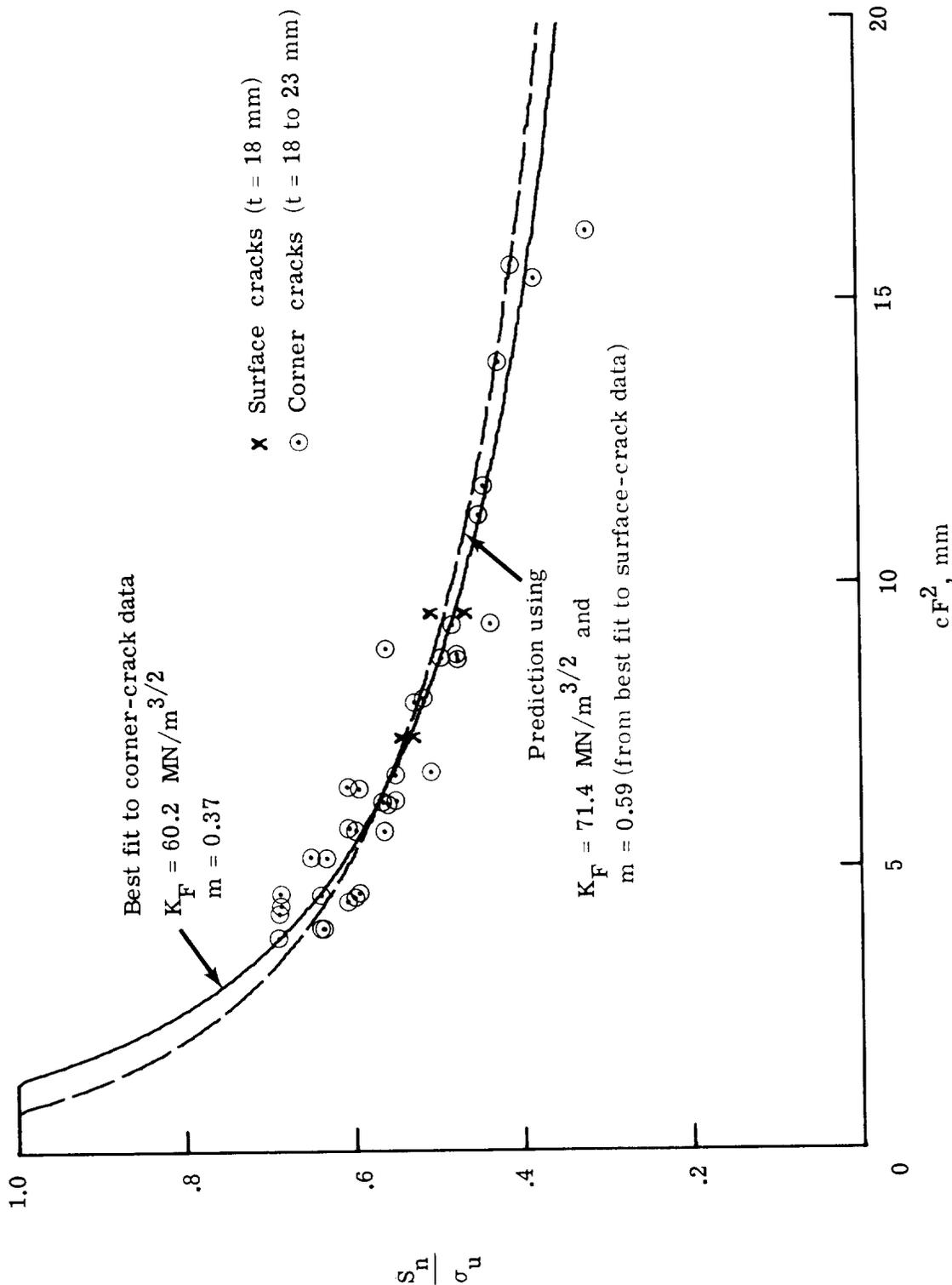
Figure 4.- Comparison of experimental data with predicted nominal failure stresses from surface-crack fracture data for corner-crack specimens of 2219-T87 aluminum alloy. $\sigma_{ys} = 455$ MPa; $\sigma_u = 600$ MPa; T = 77 K.

26

Figure 5.- Calculated and experimental surface-crack fracture data for 2024-T3 aluminum alloy (ref. 9).

$\sigma_{ys} = 355$ MPa; $\sigma_u = 485$ MPa; room temperature.

Figure 6.- Experimental data and predicted nominal failure stresses from surface-crack fracture data for 2024-T3 aluminum alloy (ref. 9). $\sigma_{ys} = 355$ MPa; $\sigma_u = 485$ MPa; room temperature.

28

x Surface cracks (t = 5 mm)

1.0

.8

.6

.4

.2

$\dfrac{S_n}{\sigma_u}$

0   5   10   15   20

cF^2, mm

TPFC
$K_F = 112$ MN/m$^{3/2}$
m = 0.48

Figure 7.- Calculated and experimental surface-crack fracture data for Ti-6Al-4V titanium alloy (ref. 7).

$\sigma_{ys} = 1040$ MPa; $\sigma_u = 1165$ MPa; room temperature.

29
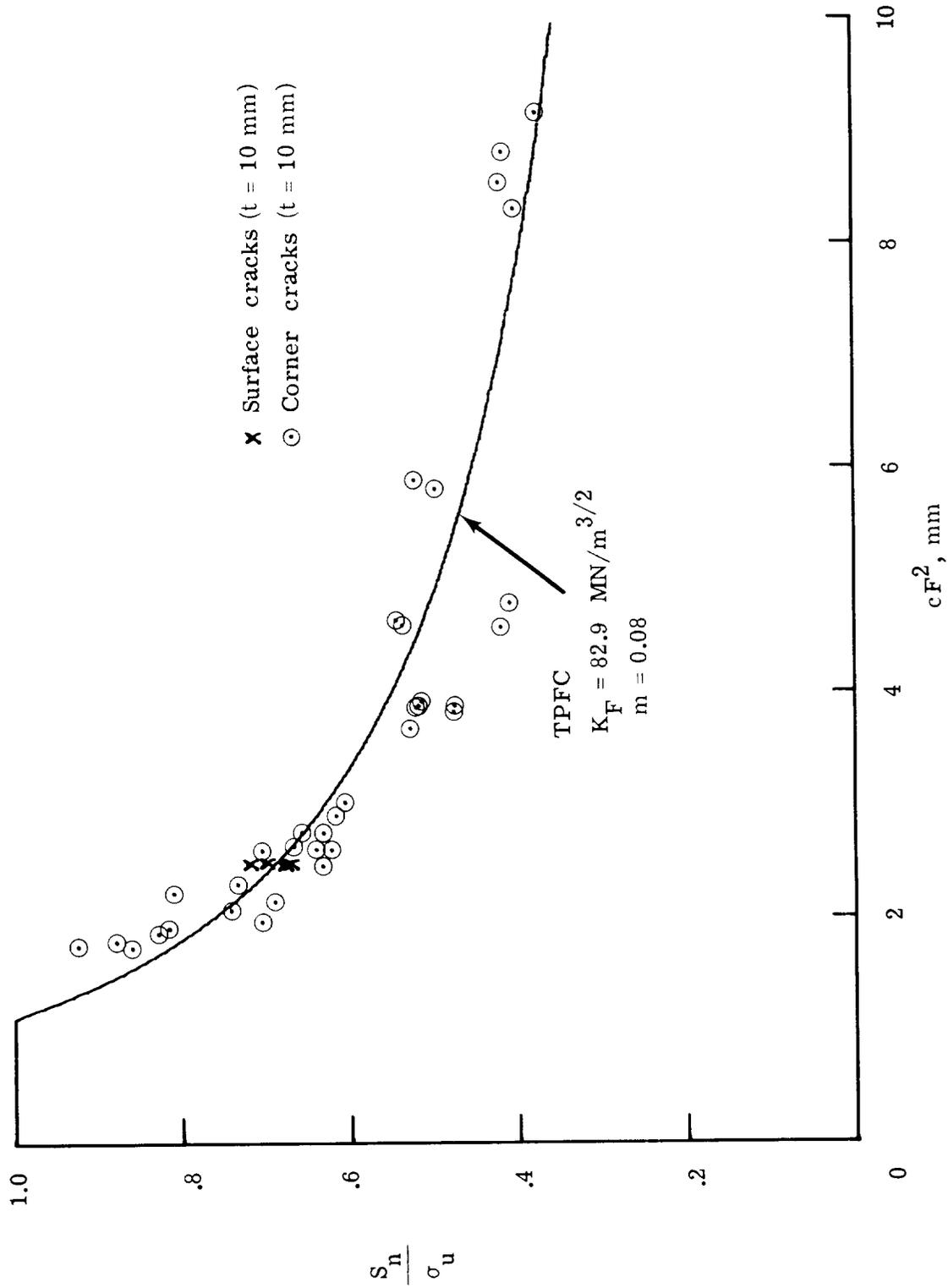
Figure 8.- Calculated and experimental surface-crack and corner-crack fracture data for Ti-5Al-2.5Sn (ELI) titanium alloy (ref. 8). $\sigma_{ys} = 1240$ MPa; $\sigma_u = 1290$ MPa; $T = 77$ K.

30
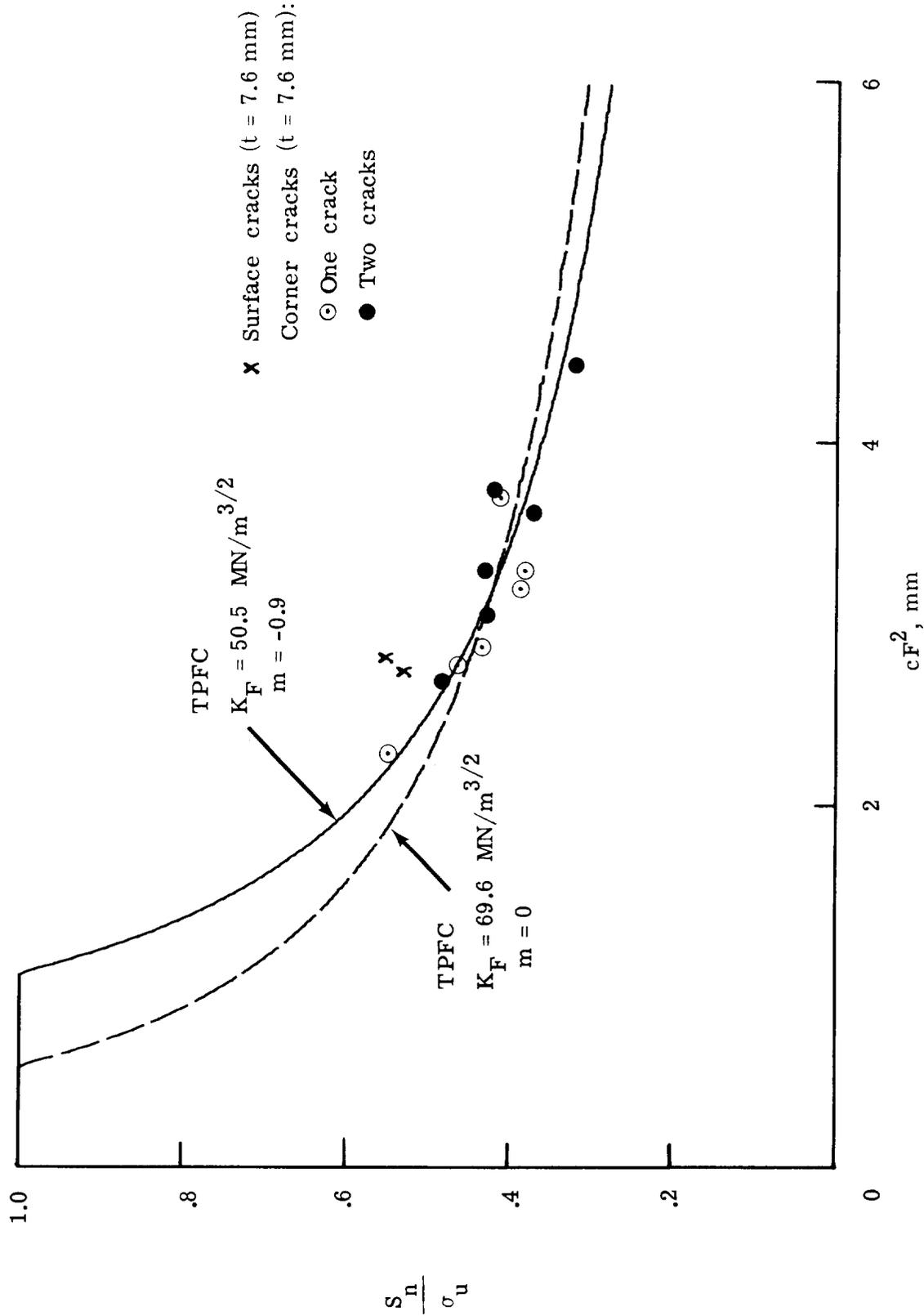
Figure 9.- Calculated and experimental surface-crack and corner-crack fracture data for 4340 steel (ref. 10). σ_{ys} = 1570 MPa; σ_u = 1650 MPa; room temperature.

31
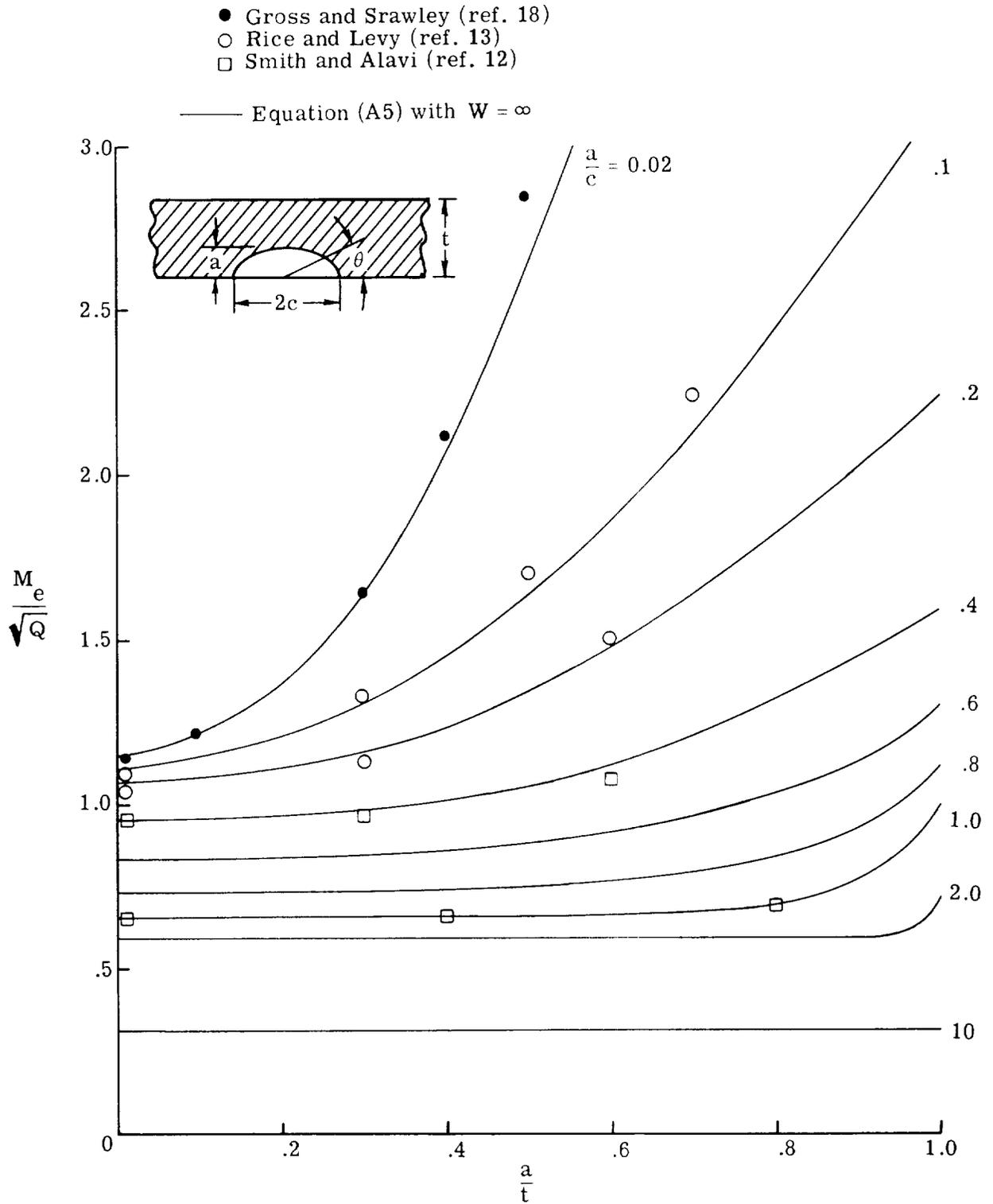
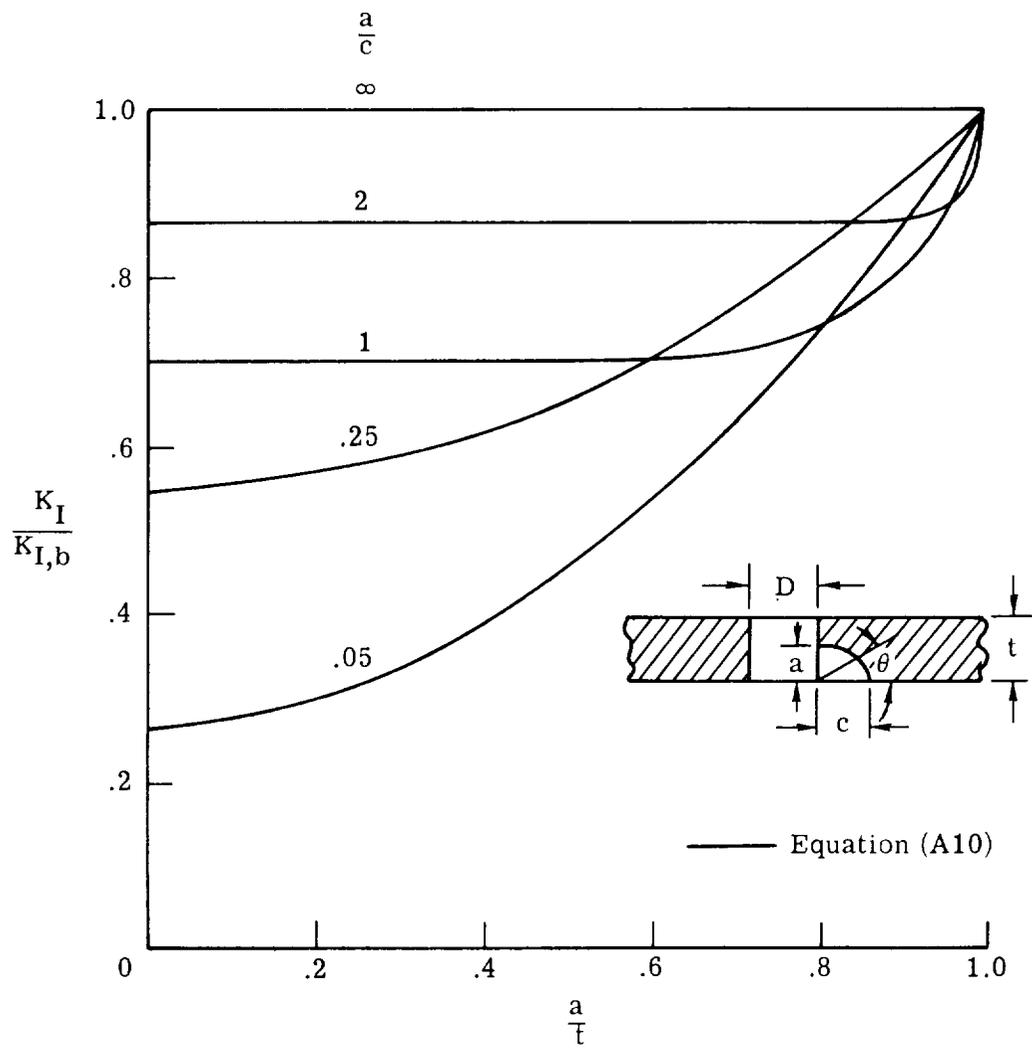Figure 10.- Boundary correction factors on stress intensity for surface crack in an infinitely wide and finite-thickness specimen.

Figure 11.- Stress-intensity factors for corner crack in an infinitely wide and finite-thickness specimen (eq. (A10)). D/t = 1; W = ∞.
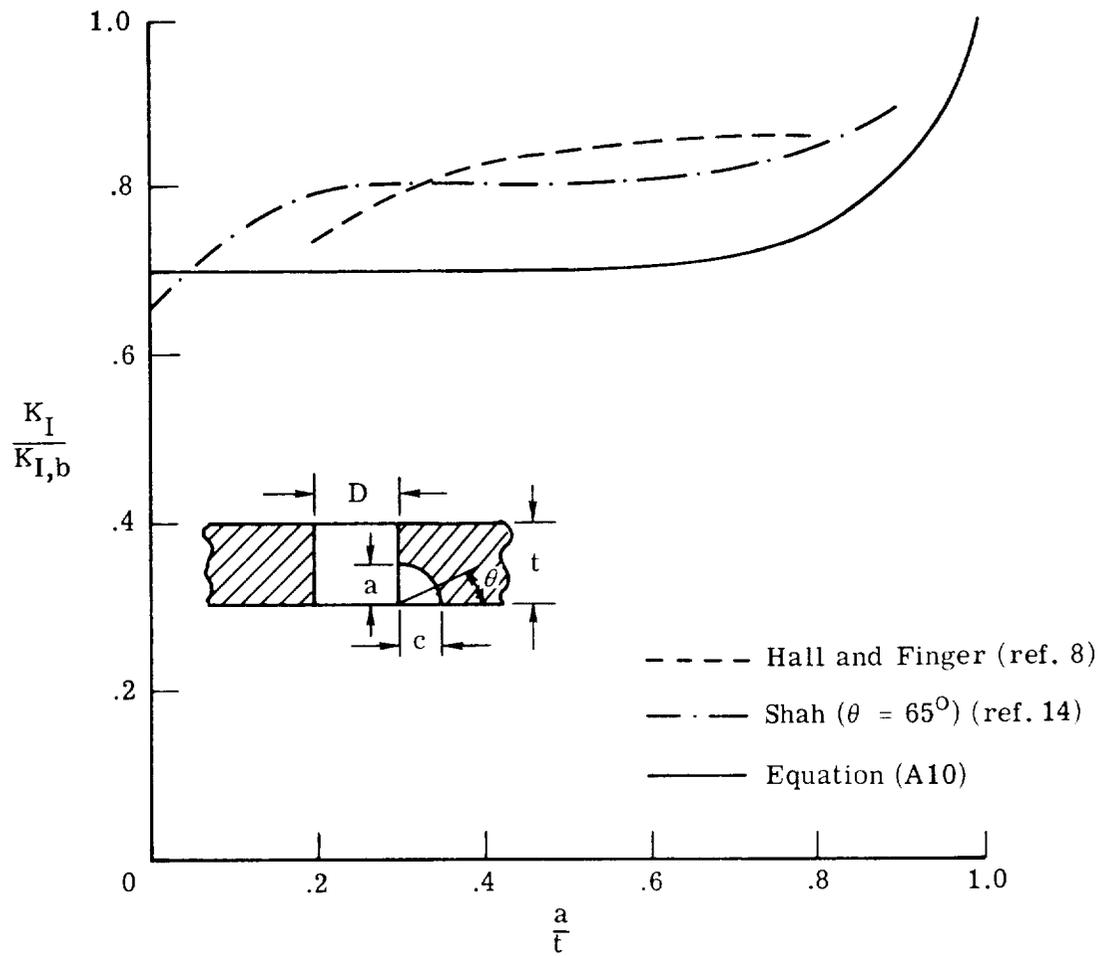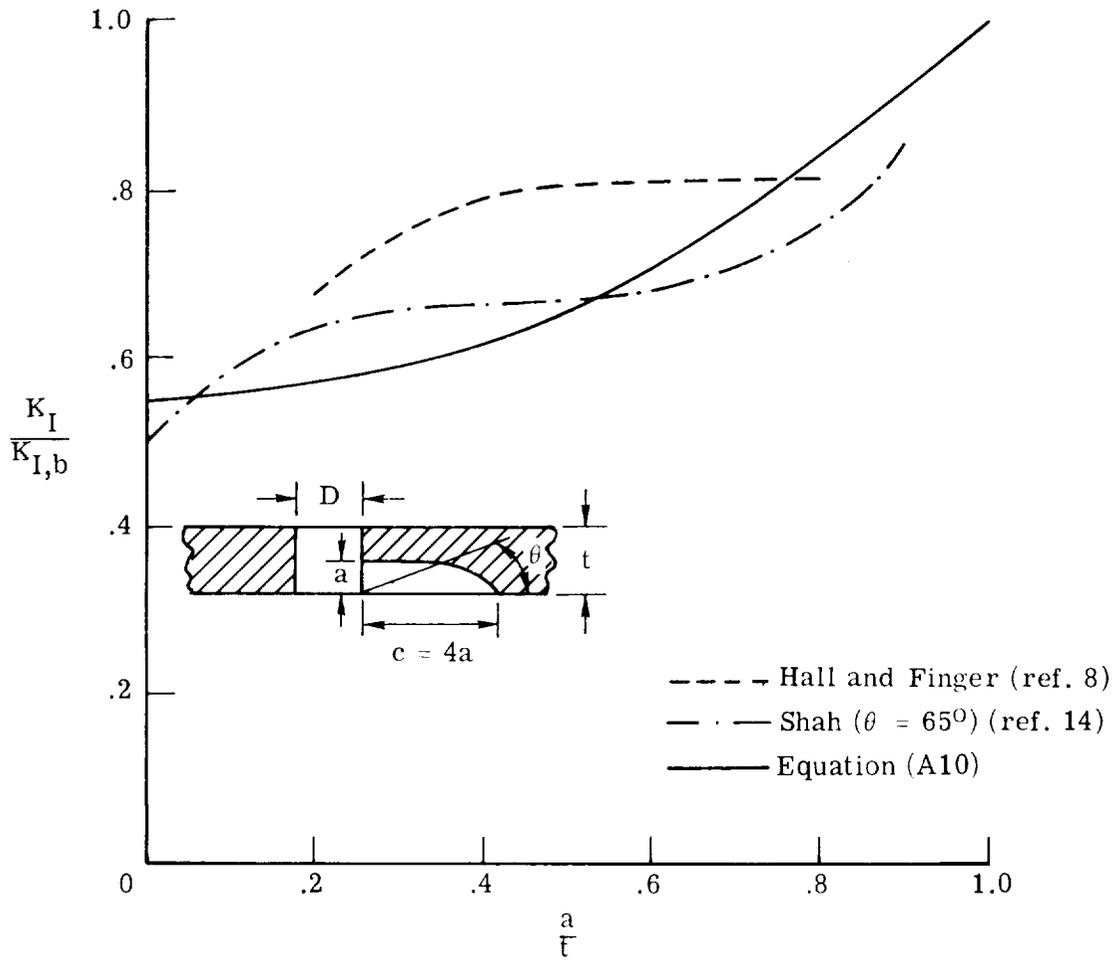
Figure 12.- Comparison of stress-intensity factors from various theories for corner crack with a/c = 1.   D/t = 1;   W = ∞.

Figure 13.- Comparison of stress-intensity factors from various theories
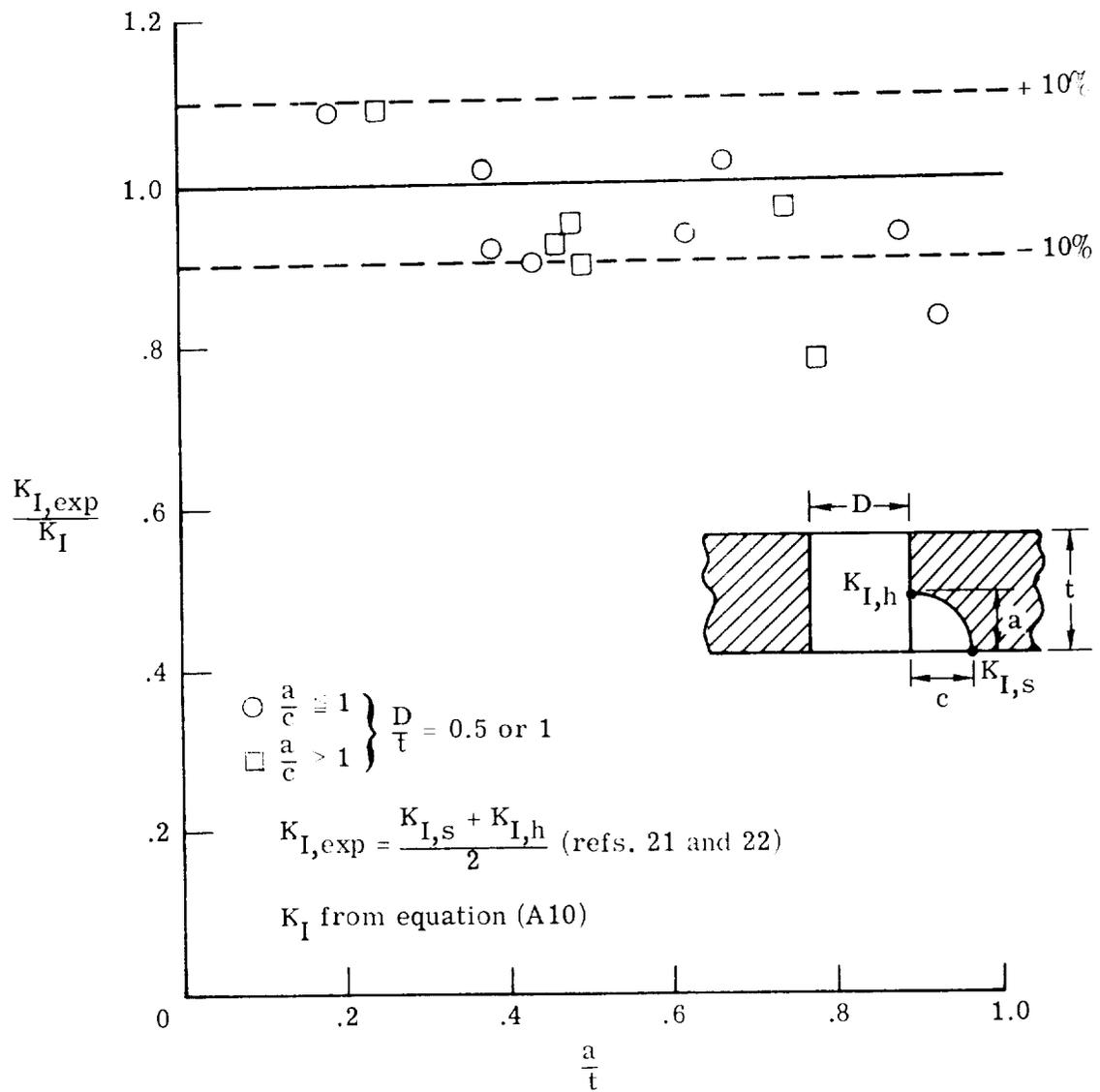for corner crack with a/c = 0.25.   D/t = 1;   W = ∞.

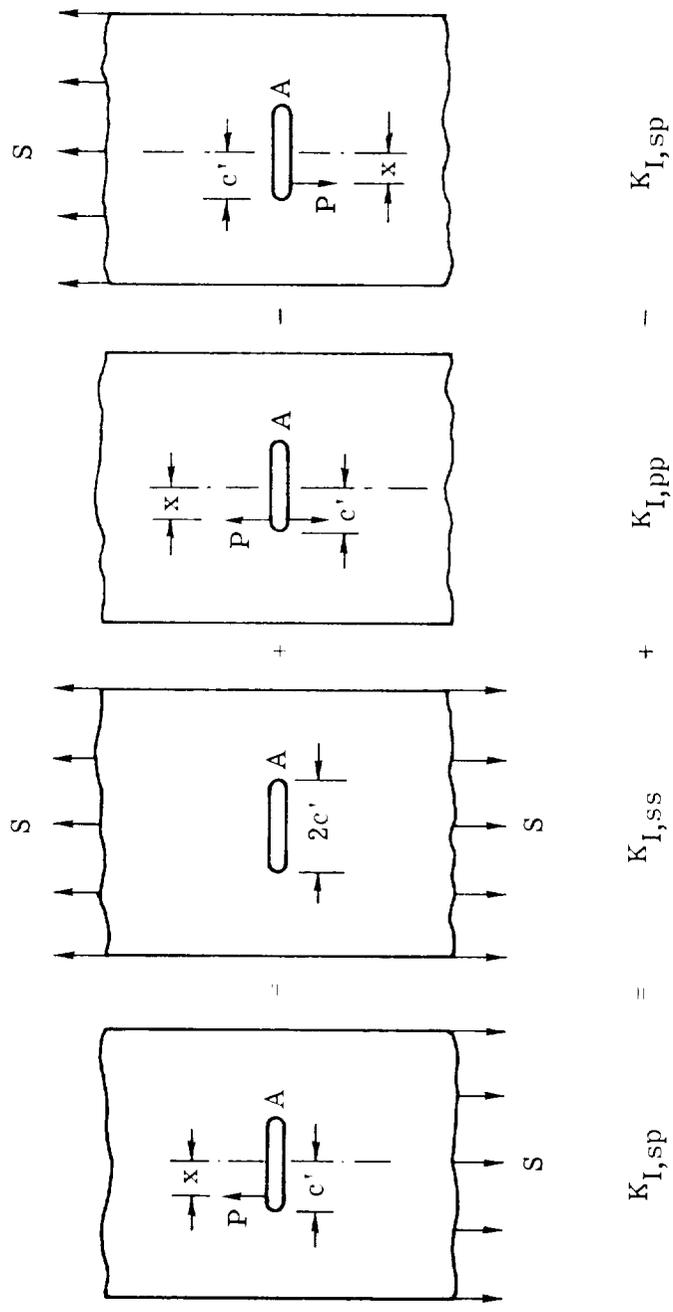Figure 14.- Comparison of experimental and theoretical stress-intensity factors for corner crack in finite plate.

Figure 15.- Stress-intensity factor at point A for single wedge-force-loaded crack obtained by superposition.

$$K_{I,sp} \quad = \quad K_{I,ss} \quad + \quad K_{I,pp} \quad - \quad K_{I,sp}$$